ISSN:2229-6107

INTERNATIONAL JOURNAL OF PURE AND APPLIED SCIENCE & TECHNOLOGY

E-mail :
editor.ijpast@gmail.com
editor@ijpast.in

www.ijpast.in

INTERNATIONAL JOURNAL OF PURE AND APPLIED SCIENCE & TECHNOLOGY
IJPAST

ISSN 2229-6107 www.ijpast.in

Vol 13,Issuse 2.May 2023

Off-board electric vehicle battery charger using PV array

[1]K. DAVID RAJU,[2]B. TULASI,[3]B. ASHRITHA,[4]K. SAI SHIVANI

ABSTRACT

During the recent decade, the automobile industry is booming with the evolution of electric vehicle (EV). Battery charging system plays a major role in the development of EVs. Charging of EV battery from the grid increases its load demand. This leads to propose a photovoltaic (PV) array-based off-board EV battery charging system in this study. Irrespective of solar irradiations, the EV battery is to be charged constantly which is achieved by employing a backup battery bank in addition to the PV array. Using the sepic converter and three-phase bidirectional DC–DC converter, the proposed system is capable of charging the EV battery during both sunshine hours and non-sunshine hours. During peak sunshine hours, the backup battery gets charged along with the EV battery and during non-sunshine hours, the backup battery supports the charging of EV battery. The proposed charging system is simulated using Simulink in the MATLAB software and an experimental prototype is fabricated and tested in the laboratory and the results are furnished in this study.

Introduction

Greenhouse emissions from traditional IC engines are having an increasingly negative impact on the environment. Because of this, the market for environmentally friendly electric cars (EVs) in the auto industry has exploded [1-3]. However, the demand for power generated by charging EV batteries from the grid rises, as do the costs to the owners of EVs who must resort to other energy sources [4, 5]. Renewable energy sources (RESs) may be utilized to charge the EV battery since they are non-polluting and will never run out. So, EVs powered by RES are a kind of "green transportation" [6]. The sun's energy is one of the most accessible RES options for charging electric vehicle batteries [7, 8]. Therefore, the suggested system makes use of power converter topologies to allow energy from a PV array to be utilized to charge the EV battery. Electric vehicles often employ lithium ion batteries because of their high power density, high efficiency, low weight, and small size [9, 10]. In addition to being able to be charged quickly, these batteries offer a long lifespan and a low self-discharge rate. The possibility of an explosion due to overcharging or a short circuit is relatively minimal. These batteries need careful voltage regulation while being charged. Electric vehicle batteries are charged using a wide variety of power electronic converters equipped with a voltage controller. The PV array's intermittent nature necessitates the use of power converters to keep the EV battery charged. In the onboard chargers of hybrid EVs, multiport converters (MPCs) are preferred due to their ability to interface various power sources and energy storage elements, such as PV arrays, ultracapacitors, super capacitors, fuel cells, and batteries, with the loads in the EV, such as the motor, lights, power windows and doors, radios, amplifiers, and mobile phone chargers. All the sources have to be installed within the EV itself, which means that MPCs add extra weight, expense, and maintenance. These converter-based EV battery charging systems enhance the complexity of controller implementation [11-13]. Since the EV battery is contained inside the vehicle unit, this study proposes an off-board charger in which the PV array and backup battery bank are situated within the charging station or parking lot.

[1]ASSISTANT PROFESSOR, [2,3&4] UG SCHOLAR
DEPARTMENT OF EEE,
MALLA REDDY ENGINEERING COLLEGE FOR WOMEN, HYDERABAD

Implementation of the Planned System

As can be seen in Fig. 1, the proposed PV-EV battery charger includes the following components: a photovoltaic array, a sepic converter, a half-bridge BIDC, an electric vehicle battery, a backup battery bank, and a controller. The consistent output voltage at the dc link is achieved by sending gate pulses from the controller to the sepic converter. Both the boost mode, in which the backup battery is charged from the PV array, and the buck mode, in which the EV battery is charged from the backup battery, need the generation of gate pulses to the switches of the BIDC. The controller is also responsible for producing the gate pulses that activate the Sa, Sb, and Sc auxiliary switches. All of the PV array's auxiliary switches, including the sepic converter, the backup battery's auxiliary switch, and the electric vehicle's auxiliary switch, are turned on when solar irradiance is high. Switch Sa is turned off to disconnect the PV array and sepic converter from the dc connection when solar irradiance is low. When the solar power is not enough to charge the backup battery, the switch Sc is set OFF to disconnect the BIDC and the backup battery from the dc connection. There are three distinct modes of operation for the proposed system, which are described below.

Mode 1

Auxiliary switches are activated to charge the EV battery and the backup battery from the PV array through the sepic converter and the BIDC, respectively, during peak sunlight hours, when the produced PV array power is greater. To charge the backup battery, the BIDC switches to forward direction operation, increasing the voltage across the dc connection.

Mode 2

The energy produced by a PV array is inadequate to fully charge an EV battery during cloudy or otherwise low-sunlight periods. Thus, with switch Sa off, the PV array is cut off from the dc connection, and switches Sb and Sc on, the EV battery is linked to the backup battery through BIDC. Here, the BIDC functions in reverse, reducing the backup battery voltage so that it may be used to charge the EV battery. 2.3 Mode 3 When the energy produced by the PV array is only enough to charge the EV battery, the dc connection between the BIDC and the backup battery bank is severed when switches Sa and Sb are turned on and switch Sc is turned off.

The suggested charger's converter design.

Sepic Convert

The sepic converter in the proposed charging system is controlled by a proportional-integral (PI) controller, which allows for a consistent output voltage regardless of the PV array voltage. As can be seen in Fig. 2, the sepic converter has a single IGBT switch, a single diode, a pair of inductors, and a pair of capacitors. Key benefits of the sepic converter include: The output voltage has the same polarity as the input voltage, unlike buck-boost and cuk converters [16], and (i) it can function in both boost and buck modes depending on the duty ratio. This equation gives us the sepic converter's voltage gain:

$$\frac{V_{dc}}{V_{PV}} = \frac{D}{1-D}$$

where Vdc is the dc link voltage, VPV is the PV array voltage and D is the duty ratio of the sepic converter. The values of inductors and capacitors of the sepic converter are chosen as per (2)–(4) [17]:

$$L_a = L_b = \frac{V_{PV_{min}} D_{max}}{2\Delta i_{PV} f_{sw}}$$

$$C_1 = \frac{I_{dc} D_{max}}{\Delta V_{C1} f_{sw}}$$

$$C_2 = \frac{I_{dc} D_{max}}{\Delta V_{dc} f_{sw}}$$

where VPVmin is the minimum PV array voltage, ΔiPV is the input current ripple, fsw is the switching frequency, Idc is the dc link

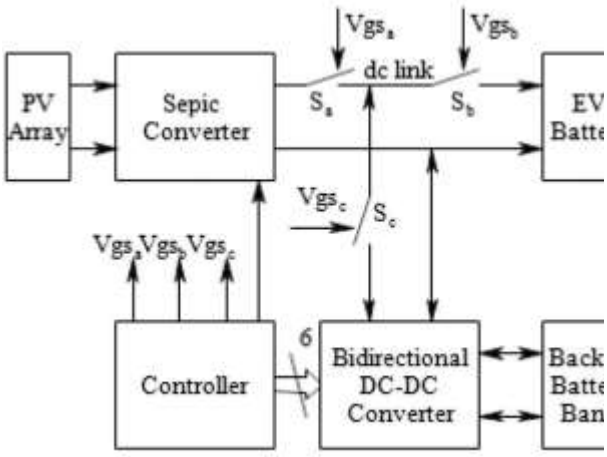

Fig. 1 Block diagram of the EV battery charger

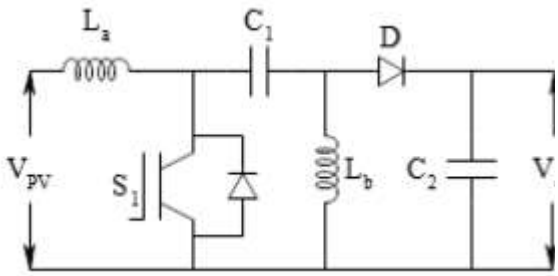

Fig. 2 Schematic diagram of sepic converter

current, ΔVC1 is the capacitor, C1 voltage ripple, ΔVdc is the output voltage ripple, and Dmax is the maximum duty ratio calculated as follows:

$$D_{max} = \frac{V_{dc} + V_D}{V_{PVmin} + V_{dc} + V_D}$$

where VD is the diode voltage drop.

Controller design

The suggested charger's controller sends gate pulses to the sepic converter's and BIDC's and auxiliary switches. Figure 4 depicts the method for activating and deactivating the auxiliary switches. The controller measures the voltage and current from the PV array and figures out the power output. The controller produces gate pulses to turn ON all the auxiliary switches to charge the EV battery and the backup battery bank concurrently from the PV array if the PV array power is higher than the EV battery rated power, PR. If the power from the PV array is less than the rated power of the EV battery but more than the minimum needed power, PM, the backup battery is disconnected from the charging system by turning off the switch Sc, and the EV battery is charged directly from the PV array by turning on switches Sa and Sb. The PV array and sepic converter are disconnected from the charging system and the switch, Sa, is closed if the power from the PV array is below the minimum needed power, PM. The EV battery will be charged from the backup power source after the switches Sb and Sc are activated. In the proposed charging system, the PI voltage controller is employed to provide gate pulses to the MOSFET in the sepic converter, which keeps the dc link voltage stable regardless of changes in the PV array voltage. Each of BIDC's three legs has two switches. The two switches in the same leg must receive gate pulses with a 180° phase difference. Based on the power from the PV array, the controller in the proposed system sends one of six gate pulses to the BIDC. If the power from the PV array is more than the power required, gate pulses are sent to the BIDC's switches, putting it into boost mode and increasing the dc link voltage to charge the backup battery bank. Gate pulses are created in this mode with a zero-degree phase for the switches in leg 1, a 120-degree phase shift for the switches in leg 2, and a 240-degree phase shift for the switches in leg 3. For BIDC operation, gate pulses are created if PV array power is below PM.

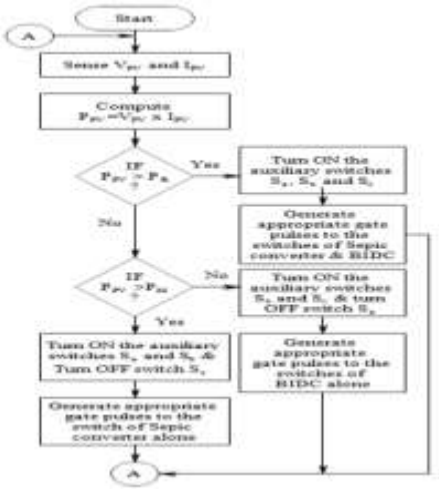

Fig. 4 Flowchart of gate pulses generation for the auxiliary switches

buck mode, producing a step down voltage at the dc link sufficient to charge the EV battery by the backup battery. In this mode, the gate pulses are fed to the leg 3 switches with 0° phase and gate pulses to the leg 2 and leg 1 switches are 120° and 240° phase shifted with respect to that of leg 3 switches, respectively.

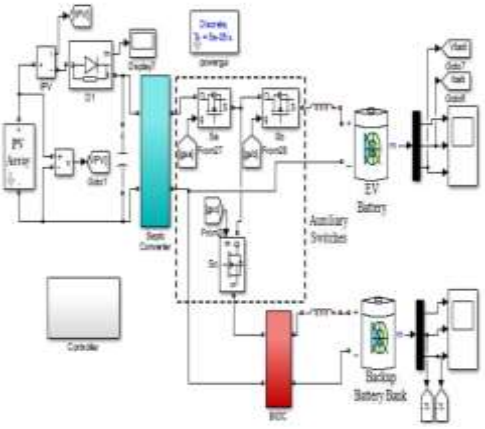

Fig. 5 Simulation model of the proposed charger

Mathematical modelling of proposed system

Mathematical model of the proposed system is obtained by combining the state-space average model of Sepic converter and Bidirectional DC–DC converter. It is derived by considering the ON and OFF switching period of the converters [26, 27]. The statespace matrices of the sepic converter, state matrix 'A', input matrix 'B', output matrix 'C', feed forward matrix 'D' are found to be

$$A = \begin{bmatrix} 0 & 0 & \frac{-(1-D_s)}{L_a} & \frac{-(1-D_s)}{L_a} \\ 0 & 0 & \frac{D_s}{L_b} & \frac{-(1-D_s)}{L_b} \\ \frac{(1-D_s)}{C_1} & \frac{-D_s}{C_1} & 0 & 0 \\ \frac{(1-D_s)}{C_2} & \frac{(1-D_s)}{C_2} & 0 & \frac{-1}{C_2 R_{eq}} \end{bmatrix}$$

$$B = \begin{bmatrix} \frac{1}{L_a} \\ 0 \\ 0 \\ 0 \end{bmatrix}$$

$$C = [0 \quad 0 \quad 0 \quad 1]$$

$$D = [0]$$

where Req is equivalent impedance at the dc link and Ds is the duty ratio of Sepic converter. Similarly, the state-space matrices of the BIDC, state matrix 'A1 ', input matrix 'B1 ', output matrix 'C1 ', feed forward matrix 'D1 ' are found to be

$$A_1 = \begin{bmatrix} \frac{-(R_{lp}+R_{dson})}{L} & 0 & \frac{-(1-D_{BIDC})}{L} \\ \frac{-1+2D_{BIDC}}{C_L} & 0 & 0 \\ \frac{(1-D_{BIDC})}{C_H} & 0 & \frac{-1}{C_H R_{eq1}} \end{bmatrix}$$

$$B_1 = \begin{bmatrix} \frac{1}{L} \\ 0 \\ 0 \end{bmatrix}$$

$$C_1 = [0 \quad 0 \quad 1]$$

$$D_1 = [0]$$

RL1 is the parasitic resistance of inductor L1, L = (L1/3)Rlp, Req1 is the equivalent impedance across capacitor CH, Rdson is the MOSFET turn on resistance, and DBIDC is the duty ratio of BIDC. The total transfer function of the proposed system is calculated by combining the transfer functions of the converters, which are computed using the aforementioned state-space models. The suggested system is stable, as shown by the positive gain margin and phase margin seen in the frequency response. The next part presents the findings of simulation experiments performed on the suggested charger.

MPC

Model predictive control (MPC) is an advanced method of process control that is used to control a process while satisfying a set of constraints. It has been in use in the process industries in chemical plants and oil refineries since the 1980s. In recent years it has also been used in power system balancing models[1] and in power electronics.[2] Model predictive controllers rely on dynamic models of the process, most often linear empirical models obtained by system identification. The main advantage of MPC is the fact that it allows the current timeslot to be optimized, while keeping future timeslots in account. This is achieved by optimizing a finite time-horizon, but only implementing the current timeslot and then optimizing again, repeatedly, thus differing from a linear–quadratic regulator (LQR). Also MPC has the ability to anticipate future events and can take control actions accordingly. PID controllers do not have this predictive ability. MPC is nearly universally implemented as a digital control, although there is research into achieving faster response times with specially designed analog circuitry.[3] Generalized predictive control (GPC)

and dynamic matrix control (DMC) are classical examples of MPC.

Overview

The models used in MPC are generally intended to represent the behavior of complex and simple dynamical systems. The additional complexity of the MPC control algorithm is not generally needed to provide adequate control of simple systems, which are often controlled well by generic PID controllers. Common dynamic characteristics that are difficult for PID controllers include large time delays and high-order dynamics.

MPC models predict the change in the dependent variables of the modeled system that will be caused by changes in the independent variables. In a chemical process, independent variables that can be adjusted by the controller are often either the setpoints of regulatory PID controllers (pressure, flow, temperature, etc.) or the final control element (valves, dampers, etc.). Independent variables that cannot be adjusted by the controller are used as disturbances. Dependent variables in these processes are other measurements that represent either control objectives or process constraints.

MPC uses the current plant measurements, the current dynamic state of the process, the MPC models, and the process variable targets and limits to calculate future changes in the dependent variables. These changes are calculated to hold the dependent variables close to target while honoring constraints on both independent and dependent variables. The MPC typically sends out only the first change in each independent variable to be implemented, and repeats the calculation when the next change is required.

While many real processes are not linear, they can often be considered to be approximately linear over a small operating range. Linear MPC approaches are used in the majority of applications with the feedback mechanism of the MPC compensating for prediction errors due to structural mismatch between the model and the process. In model predictive controllers that consist only of linear models, the superposition principle of linear algebra enables the effect of changes in multiple independent variables to be added together to predict the response of the dependent variables. This simplifies the control problem to a series of direct matrix algebra calculations that are fast and robust.

When linear models are not sufficiently accurate to represent the real process nonlinearities, several approaches can be used. In some cases, the process variables can be transformed before and/or after the linear MPC model to reduce the nonlinearity. The process can be controlled with nonlinear MPC that uses a nonlinear model directly in the control application. The nonlinear model may be in the form of an empirical data fit (e.g. artificial neural networks) or a high-fidelity dynamic model based on fundamental mass and energy balances. The nonlinear model may be linearized to derive a Kalman filter or specify a model for linear MPC.

An algorithmic study by El-Gherwi, Budman, and El Kamel shows that utilizing a dual-mode approach can provide significant reduction in online computations while maintaining comparative performance to a non-altered implementation. The proposed algorithm solves N convex optimization problems in parallel based on exchange of information among controllers.

Principles of MPC

Model predictive control is a multivariable control algorithm that uses:

an internal dynamic model of the process

a cost function J over the receding horizon

an optimization algorithm minimizing the cost function J using the control input u

Nonlinear MPC

Nonlinear model predictive control, or NMPC, is a variant of model predictive control that is characterized by the use of nonlinear system models in the prediction. As in linear MPC, NMPC requires the iterative solution of optimal control problems on a finite prediction horizon. While these problems are convex in linear MPC, in nonlinear MPC they are not necessarily convex anymore. This poses challenges for both NMPC stability theory and numerical solution.[8]

The numerical solution of the NMPC optimal control problems is typically based on direct optimal control methods using Newton-type optimization schemes, in one of the variants: direct single shooting, direct multiple shooting methods, or direct collocation.[9] NMPC algorithms typically exploit the fact that consecutive optimal control problems are similar to each other. This allows to initialize the Newton-type solution

procedure efficiently by a suitably shifted guess from the previously computed optimal solution, saving considerable amounts of computation time. The similarity of subsequent problems is even further exploited by path following algorithms (or "real-time iterations") that never attempt to iterate any optimization problem to convergence, but instead only take a few iterations towards the solution of the most current NMPC problem, before proceeding to the next one, which is suitably initialized; see, e.g.,.[10]. Another promising candidate for the nonlinear optimization problem is to use a randomized optimization method. Optimum solutions are found by generating random samples that satisfy the constraints in the solution space and finding the optimum one based on cost function. [11]

While NMPC applications have in the past been mostly used in the process and chemical industries with comparatively slow sampling rates, NMPC is being increasingly applied, with advancements in controller hardware and computational algorithms, e.g., preconditioning,[12] to applications with high sampling rates, e.g., in the automotive industry, or even when the states are distributed in space (Distributed parameter systems).[13] As an application in aerospace, recently, NMPC has been used to track optimal terrain-following/avoidance trajectories in real-time

Explicit MPC

Explicit MPC (eMPC) allows fast evaluation of the control law for some systems, in stark contrast to the online MPC. Explicit MPC is based on the parametric programming technique, where the solution to the MPC control problem formulated as optimization problem is pre-computed offline.[15] This offline solution, i.e., the control law, is often in the form of a piecewise affine function (PWA), hence the eMPC controller stores the coefficients of the PWA for each a subset (control region) of the state space, where the PWA is constant, as well as coefficients of some parametric representations of all the regions. Every region turns out to geometrically be a convex polytope for linear MPC, commonly parameterized by coefficients for its faces, requiring quantization accuracy analysis.[16] Obtaining the optimal control action is then reduced to first determining the region containing the current state and second a mere evaluation of PWA using the PWA coefficients stored for all regions. If the total number of the regions is small, the implementation of the eMPC does not require significant computational resources (compared to the online MPC) and is uniquely suited to control systems with fast dynamics.[17] A serious drawback of eMPC is exponential growth of the total number of the control regions with respect to some key parameters of the controlled system, e.g., the number of states, thus dramatically increasing controller memory requirements and making the first step of PWA evaluation, i.e. searching for the current control region, computationally expensive.

Results from investigations using simulation

The suggested system is simulated in the MATLAB software package, specifically in the Simulink environment. The classical equation for a PV array is used for modeling purposes [28, 29]. Power MOSFETs, inductors, and capacitors from the SimPowerSystems Blockset in the simulink library are used to mimic the Sepic and BIDC converter. The controller is built using components from the Simulink library, including a PWM generator, a pulse generator, logic gates, a comparator, a multiplier, and a PI controller. The model of a PV array is combined with

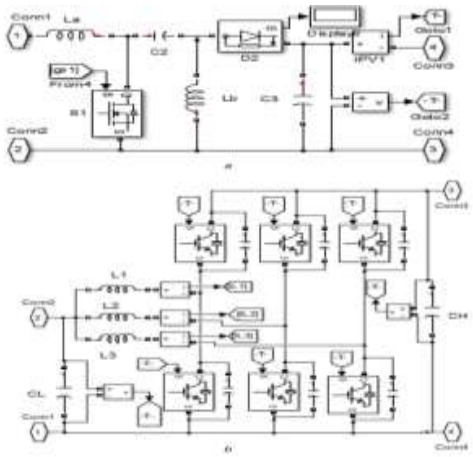

Fig. 6 Simulation model of (a) Sepic converter, (b) BIDC

developed sepic converter and BIDC along with the battery models available in Simulink library for developing the proposed charging system as shown in Fig. 5. The developed simulation model of sepic converter and BIDC shown as subsystems in Fig. 5 are depicted in Figs. 6a and b, respectively. The dynamic response of the system was investigated using the developed simulation model for PV array irradiation of 850, 100 and 500 W/m2 in mode 1, mode 2 and mode 3, respectively. The simulation results showing PV array voltage and current waveforms along with the gate pulses to the auxiliary switches are depicted in Fig. 7. Irradiation

waveforms are shown in the scale of 1 for 1000 W/m2 in Fig. 7. Thus, both EV battery and backup battery gets charged simultaneously in this mode. Whereas at low irradiation of 100 W/m2 , the gate pulses of auxiliary switches, Vgsb and Vgsc are high and gate pulse, Vgsa is low as PV array power is insufficient for charging EV battery. Thus, the backup battery

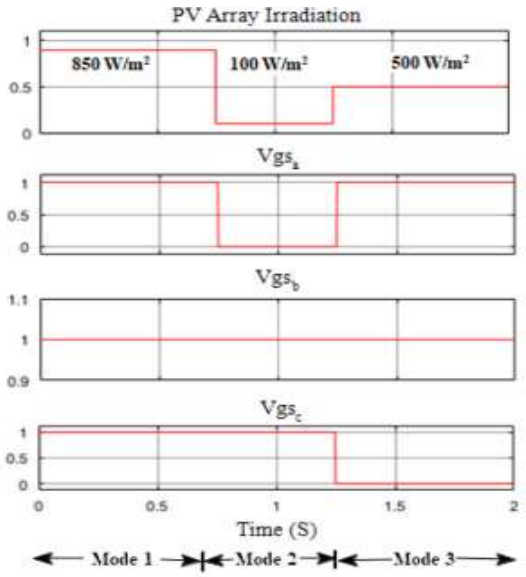

Fig. 7 Waveforms of PV array irradiation and gate pulses to the auxiliary switches

Switch Sb off to stop the charging system from trickle charging the EV battery. The dynamic waveforms of the PV array, dc link, electric vehicle battery, and backup battery are shown in Fig. 8 at the corresponding irradiation levels. As can be seen in Figs. 8a and b, the sepic converter is used to reduce the 33.3 V PV array voltage, VPV, to the 28 V dc link voltage, Vdc, in mode 1. As demonstrated in Fig. 8c, the EV battery's state of charge (SOC) increases while its negative current increases during this charging mode. In this mode, as shown in Fig. 8d, the BIDC acts as a boost converter in the forward direction, increasing the dc link voltage, Vdc, from 28 to 60.6 V in order to charge the backup battery while maintaining a constant SOC. Figure 8a shows the voltage and current waveforms of the PV array in mode 2 (during non-sunny hours and low irradiation circumstances), with the PV array voltage, VPV, increasing to its open circuit voltage of 37.25 V and the PV array current, IPV, being 0 A. During this time, as seen in Fig. 8c, the BIDC functions in buck mode in reverse direction, reducing the voltage from the secondary battery to 27.32 V in order to charge the EV battery. The backup battery is being depleted, as seen by the positive current and falling SOC in Fig. 8d. when seen in Fig. 8d, the backup battery voltage drops from 60.6 V to 55.2 V when this mode concludes. Alternatively, in mode 3, the EV battery is charged with a dc link voltage, Vdc, of 27.6 V, as illustrated in Figs. 8a and b. The PV array voltage, VPV, is 31.81 V. Even in this mode, the EV battery's state of charge (SOC) is rising and the current is negative, showing that the battery is being charged. As illustrated in Fig. 8d, the backup battery's voltage stays at 55.2 V even if its current drops to zero while in mode 3, which occurs when the battery is disconnected from the charging system. In all three modes shown in Fig. 8c, the SOC of the EV battery is growing and its current is negative, indicating that the EV battery is always being charged, either by the PV array or by the backup battery.

Figure 9 depicts the waveforms of the currents flowing through the inductors of a BIDC in each of its modes of operation. The backup battery is depleted in mode 2 as seen by the direction change in the inductor current, whereas mode 1 has no inductor current at all.

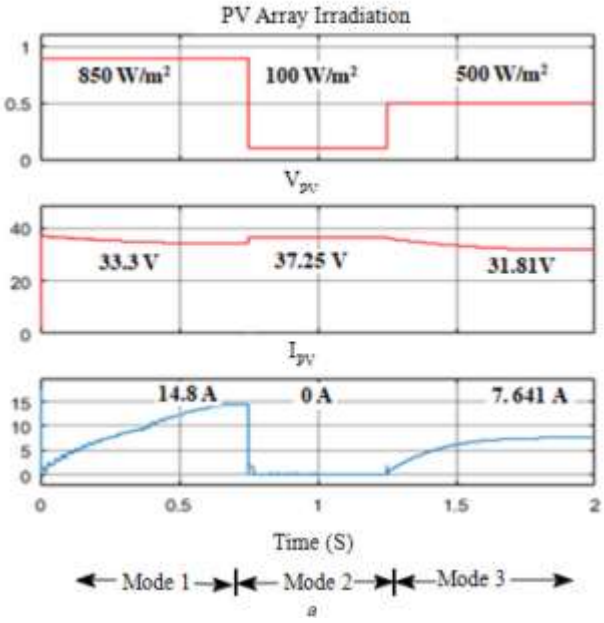

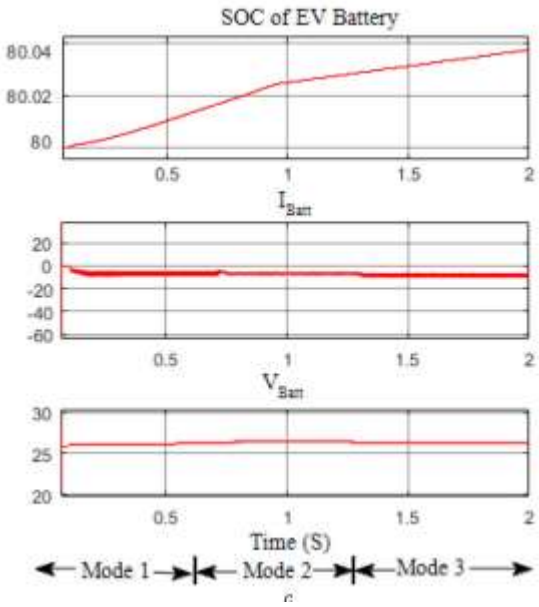

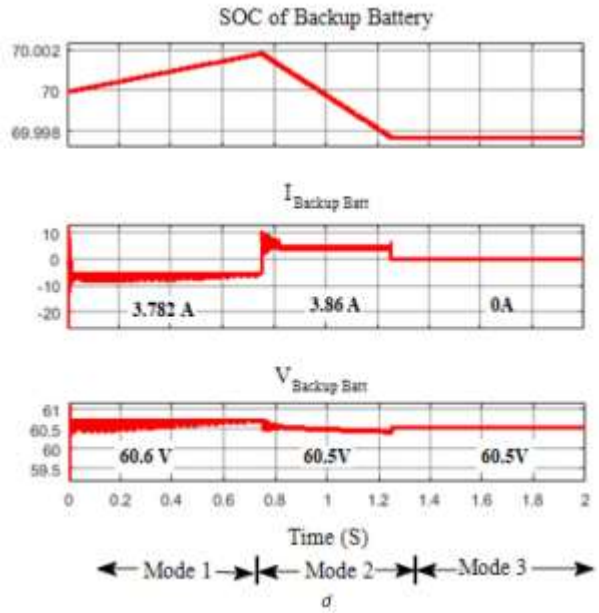

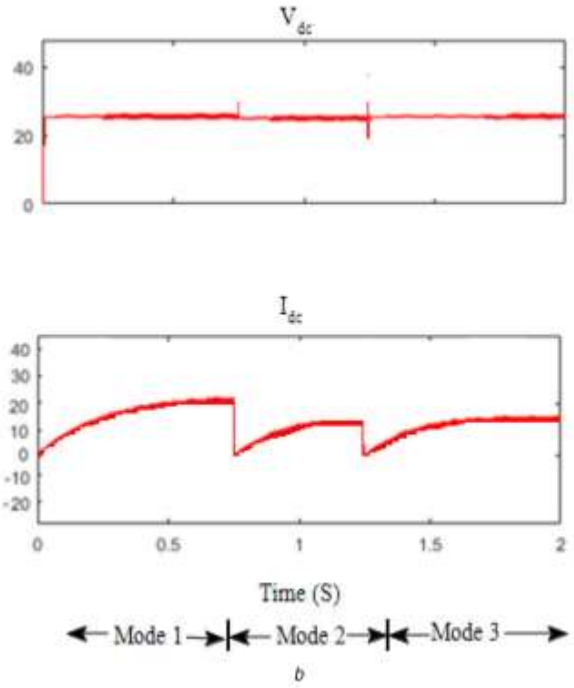

Fig. 8 Voltage (a) and current (b) waveforms at the PV array and DC connection, respectively. (c) State of Charge, Voltage, and Current of Electric Vehicle Batteries If the BIDC is not connected to the charger, the State of Charge (SOC), Current (IBackup Batt), and Voltage (VBackup Batt) of the backup battery will all read 3. In order to verify the findings of the simulation studies, a physical prototype is created and tested, with the results shown below.Methodology and Outcomes of an Experiment.The suggested electric vehicle battery charger's hardware prototype was built and tested in the lab. Input power for the experiment came from a Magna programmable dc supply, which was used to power a PV array (consisting of two panels with an open circuit voltage, Voc, of 37.25 V and a short circuit current, Isc, of 8.75 A). The components needed to build a sepic converter are the 100 V, 28 A MOSFET IRF540, the 1200 V, 30 A diode RHRP30120, the 1 mH/20 A inductor, the 1000 F/250 V capacitor, and the 600 F/150 V capacitor. Similar MOSFETs, 0.1 F/63 V snubber capacitors, 85 H/15 A inductors, and 1 F/450 V capacitors are used to construct a BIDC.

F and 160 V and 100 F/V. Using a PIC16F876A microcontroller and an IR2130 driver circuit, switching frequency of 25 kHz is sent to the MOSFET switches of the sepic converter and the BIDC. Two lead acid batteries (12 V, 35 Ah) in series serve as the EV's power source, while five lead acid batteries (12 V, 100 Ah) in series serve as the system's redundancy. Table 1 provides the technical specifications for the proposed system's components. The OPAL-RT Real time simulator OP4500 is used for the experimental inquiry, which

is conducted using a rapid control prototyping (RCP) technique. The RT Lab environment utilizes the MATLAB/Simulink software package for the controller's development. Vin and Iin are measured by a sensing instrument in the lab and sent into the controller as analogue input through the OP4500's DB37-connected analogue input ports. OPAL-RT's analogue output ports carry the gate pulses used to control the MOSFET switches through the IR2130 driver circuit.

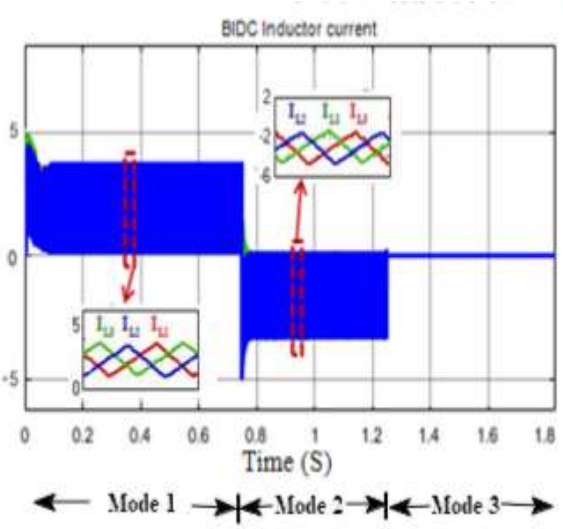

Fig. 9 Inductor current waveforms of BIDC

Conclusion

In this study, we suggest a PV array-fed off-board method for charging electric vehicle batteries. This article explains how the system can adapt to different irradiation circumstances in order to charge the EV battery continuously. The MATLAB software's Simulink environment is used for the system's design and simulation. Prototype hardware is built and tested in the lab for each of the three modes of operation of the proposed charging system. Experimental examination is performed using RCP approach in OPAL-RT Real time simulator OP4500, and the dynamic response of the system is provided using both methods. The efficacy of the suggested charger is shown by the agreement between the simulation and experimental findings.

References

[1] Santhosh, T.K., Govindaraju, C.: 'Dual input dual output power converter with one-step-ahead control for hybrid electric vehicle applications', IET Electr. Syst. Transp., 2017, 7, (3), pp. 190–200

[2] Shukla, A., Verma, K., Kumar, R.: 'Voltage-dependent modelling of fast charging electric vehicle load considering battery characteristics', IET Electr. Syst. Transp., 2018, 8, (4), pp. 221–230

[3] Wirasingha, S.G., Emadi, A.: 'Pihef: plug-in hybrid electric factor', IEEE Trans. Veh. Technol., 2011, 60, pp. 1279–1284

[4] Kirthiga, S., Jothi Swaroopan, N.M.: 'Highly reliable inverter topology with a novel soft computing technique to eliminate leakage current in grid-connected transformerless photovoltaic systems', Comput. Electr. Eng., 2018, 68, pp. 192–203

[5] Badawy, M.O., Sozer, Y.: 'Power flow management of a grid tied PV-battery system for electric vehicles charging', IEEE Trans. Ind. Appl., 2017, 53, pp. 1347–1357

[6] Van Der Meer, D., Chandra Mouli, G.R., Morales-Espana Mouli, G., et al.: 'Energy management system with PV power forecast to optimally charge EVs at the workplace', IEEE Trans. Ind. Inf., 2018, 14, pp. 311–320

[7] Xavier, L.S., Cupertino, A.F., Pereira, H.A.: 'Ancillary services provided by photovoltaic inverters: single and three phase control strategies', Comput. Electr. Eng., 2018, 70, pp. 102–121 [8] Krithiga, S., Ammasai Gounden, N.: 'Investigations of an improved PV system topology using multilevel boost converter and line commutated inverter with solutions to grid issues', Simul. Model. Pract. Theory, 2014, 42, pp. 147–159

[9] Sujitha, N., Krithiga, S.: 'RES based EV battery charging system: a review', Renew. Sustain. Energy Rev., 2017, 75, pp. 978–988

[10] Farzin, H., Fotuhi-Firuzabad, M., Moeini-Aghtaie, M.: 'A practical scheme to involve degradation cost of lithium-ion batteries in vehicle-to-grid applications', IEEE Trans. Sustain. Energy, 2016, 7, pp. 1730–1738

[11] Zubair, R., Ibrahim, A., Subhas, M.: 'Multiinput DC–DC converters in renewable energy applications – an overview', Renew. Sustain. Energy Rev., 2015, 41, pp. 521–539

[12] Duong, T., Sajib, C., Yuanfeng, L., et al.: 'Optimized multiport dc/dc converter for vehicle drive trains: topology and design optimization', Appl. Sci., 2018, 1351, pp. 1–17

[13] Santhosh, T.K., Natarajan, K., Govindaraju, C.: 'Synthesis and implementation of a multi-port dc/dc converter for hybrid electric vehicles', J. Power Electron., 2015, 15, (5), pp. 1178–1189

[14] Hongfei, W., Peng, X., Haibing, H., et al.: 'Multiport converters based on integration of full-bridge and bidirectional dc–dc topologies for renewable generation systems', IEEE Trans. Ind. Electron., 2014, 61, pp. 856–869

[15] Shi, C., Khaligh, A.: 'A two-stage three-phase integrated charger for electric vehicles with dual cascaded control strategy', IEEE J. Emerging Sel. Topics Power Electron., 2018, 6, (2), pp. 898–909

[16] Chiang, S.J., Shieh, H., Chen, M.: 'Modeling and control of PV charger system with SEPIC converter', IEEE Trans. Ind. Electron., 2009, 56, (11), pp. 4344–4353

[17] Falin, J.: 'Designing DC/DC converters based on SEPIC topology', Analog Appl. J., 2008, 4Q, pp. 18–23. Available at https://e2echina.ti.com/cfs-file/ __key/telligent-evolution-components-attachments/ 13-112-00-00-00-00-58-20/Designing-DC-DC-converters-based-on-SEPICtopology.pdf

[18] Banaei, M.R., Sani, S.G.: 'Analysis and implementation of a new SEPICbased single-switch buck–boost DC–DC

converter with continuous input current', IEEE Trans. Power Electron., 2018, 33, (12), pp. 10317–10325

[19] Singh, A.K., Pathak, M.K.: 'Single-stage ZETA-SEPIC-based multifunctional integrated converter for plug-in electric vehicles', IET Electr. Syste. Transp., 2018, 8, (2), pp. 101–111

[20] Du, Y., Zhou, X., Bai, S., et al.: 'Review of non-isolated bi-directional DCDC converters for plug-in hybrid electric vehicle charge station application at municipal parking decks'. 2010 Twenty-Fifth Annual IEEE Applied Power Electronics Conf. Exposition, Palm Springs, CA, USA., 2010, pp. 1145–1151

[21] Kwon, M., Oh, S., Choi, S.: 'High gain soft-switching bidirectional DC–DC converter for eco-friendly vehicles', IEEE Trans. Power Electron., 2014, 29, pp. 1659–1666